

An Experimental Study of Odometer as a Navigation-aid for Land Vehicle Application

G. Muralikrishna^{#,*}, G. Malleshm[§], Abhishek Jain[#] and Praveen Tiwari[#]

[#]DRDO-Directorate of Navigation, Research Centre Imarat, Hyderabad - 500 069, India

[§]Department of EE, University College of Engineering, Osmania University, Hyderabad - 500 007, India

*E-mail: mkgurram@gmail.com

ABSTRACT

Strap-down Inertial Navigation System (SINS) shall provide position, velocity, and orientation information with reference to a pre-defined reference frame. The SINS shall have excellent accuracy over a short duration and is highly self-contained. However, the errors in navigation solutions build up exponentially with time and make the system output very unstable. In order to mitigate these errors, there is a need for a damping mechanism through external aiding sensors. In this article, one such approach is proposed to improve navigation accuracy for land vehicles in the GNSS (Global Navigation Satellite Systems) denied environment. The design and implementation of an odometer are carried out with the use of inductive proximity sensors and a mounting assembly to attach the odometer to one of the non-steering wheels of a vehicle. The odometer gives the pulse-high and pulse-low output with reference to the rotation of the wheel to which it is attached. Vehicle ground velocity is derived through sensed output pulses processed through quadrature decoder circuitry. Odometer measurements along with Non-Holonomic Constraints (NHC) are used for minimizing velocity and position errors in SINS using an Extended Kalman Filter (EKF) technique. Field trials are carried out to validate the proposed scheme of hybrid navigation with odometer design and experimental results are presented with a positioning accuracy of 0.05 % of distance travelled (DT).

Keywords: Inertial navigation system; Odometer; Proximity wheel; Proximity sensor; Quadrature decoder; Extended Kalman filter

NOMENCLATURE

‘n’ : Navigation frame defined along north-east-down axes
 ‘b’ : Body frame defined forward-right-down axes of a sensor cluster
 ‘e’ : Earth-centre-earth-fixed (ECEF) frame
 f^b : Specific acceleration vector measured by accelerometers in b-frame
 dcm_n^b : Direction cosine matrix transforms vector from b-frame to n-frame.
 g_l^n : Earth gravity vector in ‘n’ frame.
 ω_{ie}^n : Earth rate vector in n-frame
 ω_{ie}^e : Earth transport rate vector in e-frame
 λ_d : Geodetic latitude,
 L_d : Longitude
 h_d : Height in WGS84 model,
 R_N : Transverse radius of Earth
 R_{ss} : Meridian radius of Earth
 v_e^n : Velocity vector in n-frame
 v_N : North component of v_e^n
 v_E : East component of v_e^n
 v_D : Down component of v_e^n
 ω_s : Schuler frequency
 Ω : Earth rate along the polar axis

δp^n : Position error vector
 δv^n : Velocity error vector
 $\delta \alpha^n$: Angle error vector
 $\delta \omega^b$: Gyro bias error vector
 δf^b : Accelerometer bias error vector
 δs_{ODO} : Odometer scale factor error
 $\delta \beta_y$: Odometer pitch angle error
 $\delta \beta_z$: Odometer yaw angle error

1. INTRODUCTION

Sensors are the most important devices to be engaged in various industrial and consumer applications. IEEE-Std-1559¹ presents data fusion towards navigation applications as the process of combining diverse types of data. Also, it defines navigation as the determination of the position, velocity, and, optionally, attitude of a vehicle in a reference coordinate system². Often, the navigation solution is obtained through different navigation techniques of which inertial navigation is well known for its autonomous and self-contained operation and does not require any external signal as it makes use of its internal inertial sensors.

The accuracy requirement for land vehicles generally varies with the application. Mars rover needs to have centimetre accuracy based on mission requirements³. Also, the military land vehicles demand an accuracy of 10 mtr with GNSS as an additional aid. SINS alone cannot meet such high-end accuracy over long endurance applications. SINS

will have time-dependent errors as a function of (t^2) and (t^3) which will further compromise the long-term accuracy of the system. Inertial navigation systems often use data fusion⁴ to combine inertial sensor outputs with the outputs of various aiding devices producing an output that is commonly referred to as a blended solution. These systems are often referred to as aided or integrated inertial navigation systems. Further, the Global Positioning System (GPS) became one of the widely used aiding sources over decades due to its ability to provide absolute navigation information which is bounded over an indefinite time. But, GPS is unable to fulfill the requirements of continuity and reliability in many situations due to signal interruption at times when it is critically required under adverse conditions like jamming and spoofing⁵. Thus, in general, GPS/GNSS cannot be solely used for navigation, especially in the battlefield, urban canyons⁶ and the thick vegetation around the moving vehicle. Hence, the researcher(s) are exploring alternative means of achieving precise positioning accuracy with several auxiliary sensors along with SINS.

Further, as per recent works reported in published literature, the SINS has been used along with other aiding sensors like Odometer, Baro-altimeter⁷, Magnetometer, LiDAR, laser Doppler velocimeter (LDV), etc for cases where GNSS is not available or completely denied. The combination of measurements of these sensors not only offers accuracy but also ensures availability due to multi-sensor-data-fusion⁸. The point cloud features of LiDAR in⁹ are exploited to generate the velocity information of the vehicle and integrated with SINS. The LiDAR is predominantly being used in autonomous ground vehicles, but the derived velocities are often noisy making it difficult to use for high-accuracy navigation applications. The combination of LDV & SINS-based integrated navigation system has shown very promising results as presented in¹⁰. Unfortunately, the LDV is prone to environmental conditions like dust and raining roads, causing the covering of optical parts of measuring instruments. Also, LDV sensing instruments are relatively costly and bulky when compared to self-contained odometer sensing assembly.

Hence, based on the limitations of above published works, the authors in the present manuscript proposed to make use of integrated measurements of wheel-mounted odometer in body frame of sensor assembly. Further, NHC based measurements are superimposed to have the hybrid navigation solution along with wheel mounted odometer as an auxiliary sensor. The motivation for the present work is to develop high accurate and high reliable integrated navigation mechanization under GNSS-denied environments for autonomous land vehicles.

The objective of the present work reported is to achieve the improved navigation accuracy of SINS with the use of odometer as an aiding sensor through multi-sensor data fusion scheme under GNSS-challenging environments. The objective of designing such high accurate navigation system is achieved by developing odometer sensor cluster along with multi-sensor data fusion through EKF. Firstly, the research work started with the development of odometer sensor cluster, sensor processing electronics followed by development of optimal state estimation process (EKF) towards data fusion. Finally, the performance of odometer sensor assembly along with SINS is demonstrated

through field experiments. Since the design is in-house and easily scalable, there is no dependency on Commercially-Off-The-Shelf (COTS) products. The customization of the present work elucidates not only the precise positioning need of vehicles of armed forces but also can be easily extended for autonomous vehicles of civilian applications. Hence, the present work is justified to be important for many practical applications for precise positioning under GNSS-denied environments.

The manuscript is organized as follows: Firstly, the problem of oscillatory behaviour in inertial navigation mechanization is well presented in section 2. Also, section 2 presents various techniques published in the literature towards the multi-sensor data fusion algorithms and the proposed method. Further, the proposed design scheme of odometer sensor assembly followed by signal processing electronics through quadrature decoder circuitry are shown in section 3. The design of the optimal state estimation algorithm through an extended Kalman filter with Non-Holonomic Constraints (NHC) is presented in section 4 for improved performance of SINS navigation outputs. Section 5 presents the field trial results and discussion. Finally, section 6 presents the conclusion and scope of further improvements.

2. INERTIAL NAVIGATION FUNCTION

The principle of operation of SINS is depicted in Fig. 1(a). SINS shall have three levels of integrations¹¹ to obtain the position vector and two levels of integrations to obtain the velocity vector. Similarly, angular rates shall be suitably integrated by means of rotation vector dynamics to obtain attitude (i.e. orientation) information. Navigation mechanization may be expressed in north-east-down (NED) 'n' frame as:

$$\dot{v}_e^n = [dcm_n^b] f^b - [2\omega_{ie}^n + \omega_{en}^e] \times v_e^n + g_l^n \quad (1)$$

ω_{ie}^n is an earth rotation rate vector expressed in a local geographic navigation frame.

$$\omega_{ie}^n = [\Omega \cos \lambda_d \quad 0 \quad -\Omega \sin \lambda_d]^T \quad (2)$$

Ω is the earth rate along the polar axis, ω_{en}^n is the earth transport rate expressed in a local geographic navigation frame and is defined as:

$$\omega_{en}^n = [L_d \cos \lambda_d \quad -\dot{\lambda}_d \quad -L_d \sin \lambda_d]^T \quad (3)$$

where,

$$\dot{L}_d = \frac{v_E}{(R_{Nd}) \cos \lambda_d} \quad (4)$$

$$\dot{\lambda}_d = \frac{v_N}{(R_{Md})} \quad (5)$$

λ_d is geodetic latitude, L_d is longitude, h_d is height in the WGS84 model, R_N is the transverse radius of the earth, R_M is the meridian radius of the earth with $R_{Md} = (R_M + h_d)$ and $R_{Nd} = (R_N + h_d)$.

Position Computation:

$$\begin{bmatrix} \dot{\lambda}_d \\ \dot{L}_d \\ \dot{h}_d \end{bmatrix} = \begin{bmatrix} \frac{1}{R_{Md}} & 0 & 0 \\ 0 & \frac{1}{\cos(\lambda_d)(R_{Nd})} & 0 \\ 0 & 0 & -1 \end{bmatrix} \begin{bmatrix} v_N \\ v_E \\ v_D \end{bmatrix} \quad (6)$$

where, v_N, v_E, v_D are the north-east-vertical components of the velocity vector (v_e^n).

Angle propagation:

$$dcm_n^b = dcm_n^b([\omega_{nb}^b X]) \tag{7}$$

where, the operator $[X]$ is the skew-symmetric matrix version of the angular rate vector ω with superscript ‘b’ as the body measured rate in the SINS body frame and compensated for the earth rate vector in the inertial frame and finally expressed in the navigation frame (‘n’-frame).

2.1 Problem of Schuler Oscillation in Horizontal Channels

In order to study the error characteristics of navigation mechanization as explained through Eqn (1), Eqn. (6) and Eqn. (7), the small signal perturbation model is considered. Further, the horizontal and vertical channels are decoupled towards simplicity in analysis. The horizontal channel error representation² of SINS is shown in Fig. 1(b) where the error in resolved components of measured specific force δf_{xb} goes through integrations to provide velocity error δv_x and position error δp_x .

The travel over earth rate is calculated by dividing the velocity error by the earth’s equatorial radius R_0 which further modifies the dcm_n^b as SINS moves along the rotation of the earth. The angle error $\delta\theta$ within dcm_n^b will tilt the reference gravity vector g_0 as $g_0\delta\theta$ generating an equivalent error after

summation of $g_0\delta\theta$ with δf_{xb} resulting in δv_x in closed loop path.

The block reduction model of the closed loop path also called as Schuler loop is shown in Fig. 1(c). Having two integrators in the closed loop path makes the δv_x oscillatory and the corresponding transfer function of the inner loop is calculated as:

$$\frac{\delta v_x}{\delta f_{xb}} = \frac{1}{s} \frac{1}{1 + \frac{g_0}{s^2 R_0}} \tag{8}$$

and the characteristic Eqn. is given by²:

$$s^2 + \frac{g_0}{R_0} = 0 \tag{9}$$

where, ‘s’ is a Laplace operator and is written as

$$s^2 + \omega_s^2 = 0 \tag{10}$$

Which represents simple harmonic motion with oscillating frequency (Schuler frequency)

$$\omega_s = \sqrt{\left(\frac{g_0}{R_0}\right)} = 0.00124 \text{ rad/s.}$$

The time period of these oscillations is ≈ 84.4 min. The pole-zero plot of the horizontal channel is shown in Fig. 2(a) where the double poles are lying on an imaginary axis making the system oscillatory. The above period of oscillation makes the system almost unstable when sensor errors are superimposed on the measurements along with errors in initial conditions. Any small error introduced during

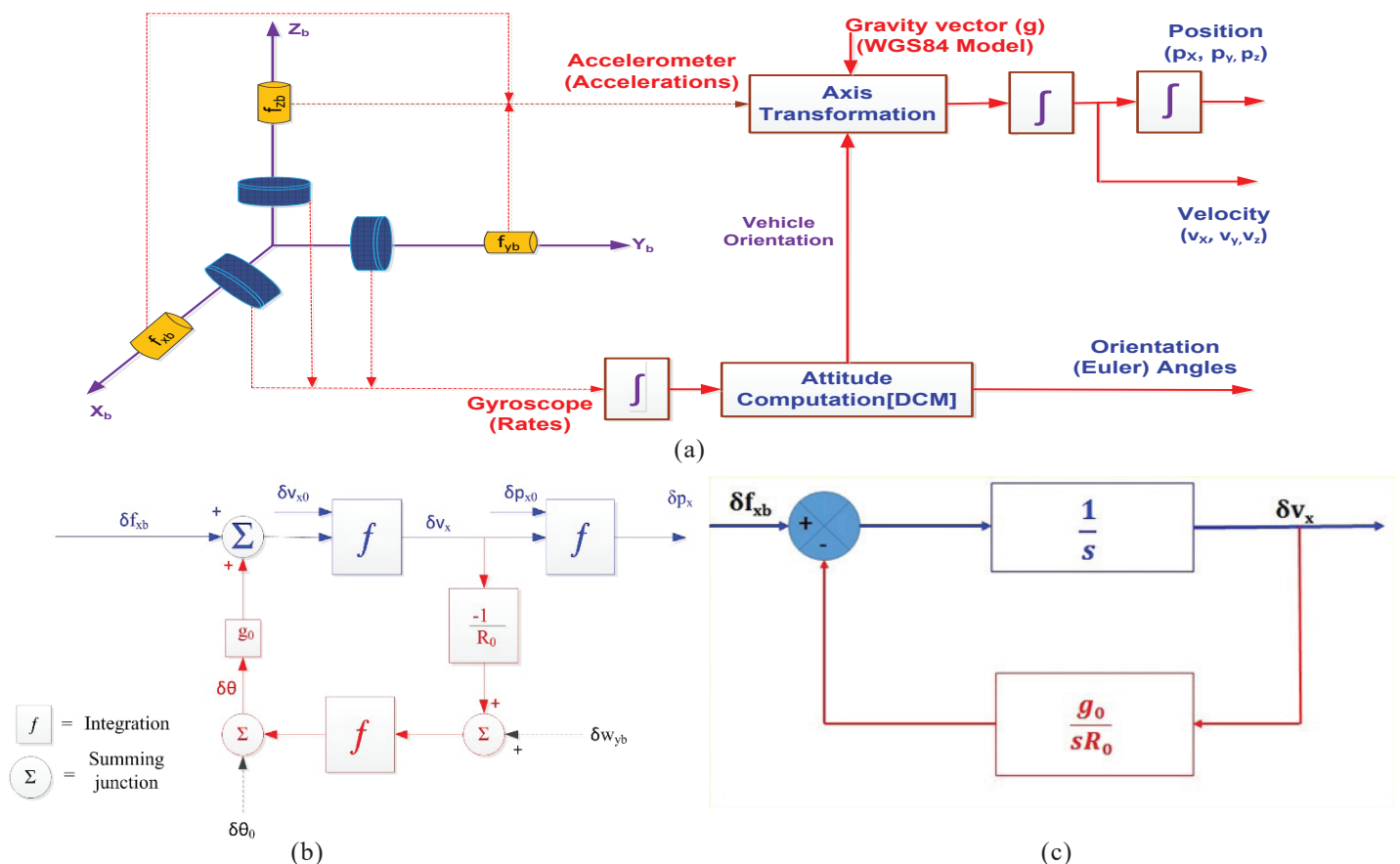


Figure 1. Position and velocity error mechanization of SINS: (a) Principle of operation of SINS; (b) Single channel (horizontal) error representation; (c) State space representation (after block reduction) of the horizontal channel.

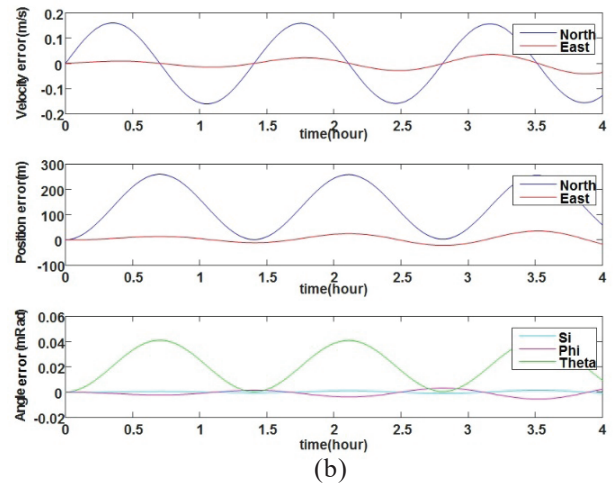
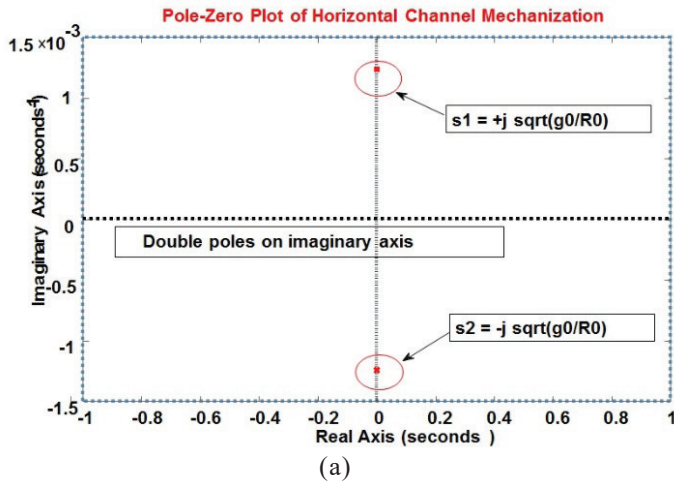


Figure 2. State space analysis of SINS: (a) Pole-Zero plot of the horizontal channel; and (b) Position, velocity, and angle errors resulting from a $10\mu\text{g}$ north accelerometer bias.

measurements shall be further integrated resulting in huge errors in position, velocity, and orientation angles over time, and the corresponding propagation of errors due to bias error of $10\mu\text{g}$ in the accelerometer is shown in Fig. 2(b). These errors have to be damped out to meet the field deployable navigation accuracies of land vehicles with an odometer as a navigation aid in an environment where GNSS is denied.

2.2 Methodology

Forward velocity measurement from the odometer is used as an aiding source towards damping of error growth in horizontal channels. As several non-linear propagations are involved in an Inertial Navigation System (INS), an extended Kalman filter (EKF) is proposed for data fusion between inertial measurements and external odometer measurements. However, to work out the improved strategy, the available literature has been studied. The methodology followed for data fusion through EKF is shown in Fig.3.

From error definition based on a common frame, the state transformation matrix-based extended Kalman filter is presented in¹² but has limitations on real-time implementation due to complexity. The authors in¹³ have tried to use the extended Kalman filter with the norm on innovation through evaluation function. A Non-Holonomic Constrained (NHC) based average speed as a measurement for the INS/Odometer integrated SINS is proposed in¹⁴. A multi-state Kalman filter¹⁵ is designed for better observability of the SINS/Doppler velocity system. But measurements are dependent on the environment and is erroneous under thick vegetation. The influence of the vehicle motion on the observability of errors in the odometer scale factor and mismatch angles are considered¹⁶⁻¹⁷. The ODO/NHC measurement models along with corner steering motion model are proposed for wheeled robots in¹⁸. However, it is not always possible to get the motion models to be embedded in a data fusion scheme, and should be very generic and free from vehicle motion models.

The concept of a multi-odo measurement model for front and rear wheels is presented in¹⁹ but the mounting of several odometers is not feasible for front wheels and further increases complexity. Wheel-mounted low grade sensor cluster is devised

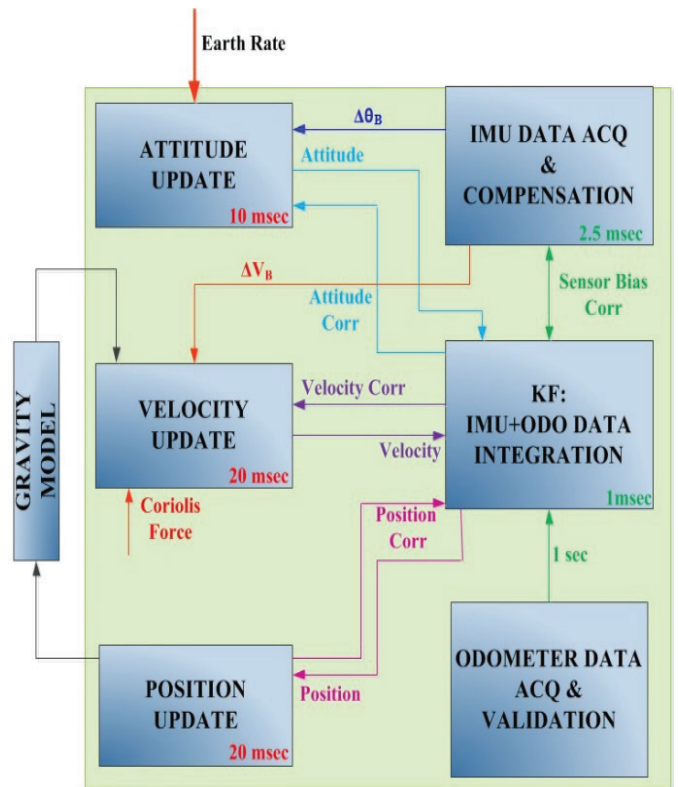


Figure 3. Proposed hybrid data fusion scheme.

in²⁰ with three types of measurements: velocity measurement, displacement increment measurement, and contact point zero-velocity measurement. However, mounting of sensor cluster on a vehicle wheel requires slip-rings to get communicated to onboard diagnostics (OBD-II) equipment and will have space constraints making it suitable for low-grade Micro-Electro-Mechanical Sensors (MEMS) only. However, all the works presented did not cover the practical design aspects of the odometer with minimum detectable pulse output as a design criterion that ensures navigation accuracy for long endurance applications. Hence, the authors in the present manuscript proposed a custom-built, in-house design of an odometer with a wide range of possible scale factors as per the type of vehicle and as per requirements of navigational accuracies. Further,

the pre-calibrated scale factor values of the odometer may vary dynamically due to the wear of the vehicle wheel over a period of time. Hence, it is proposed to estimate the scale factor of the odometer dynamically during the vehicle motion. Hence, the detailed design of the odometer assembly of navigation grade SINS with signal processing circuitry followed by an 18-state EKF is conceived in the present manuscript to estimate the navigation error state vectors as well as odometer error state vectors.

The following are the design steps involved in the proposed work:

- The design of the odometer sensing assembly
- Design of signal processing electronics and electrical pulse stream generation using proximity sensors positioned at 90 deg electrical distance.
- Calibration of the odometer sensor assembly and establishing nominal scale factor.
- Installation of odometer sensing assembly on the non-steering wheel of the land vehicle and interface with SINS.
- Design of EKF scheme and porting of navigation software on embedded System-On-Chip Processor (SOC).
- Field trials and performance validation.

Firstly, the design details of the odometer are well presented in the following section.

3. ODOMETER AND ITS SIGNAL PROCESSING

A navigation system aided by a vehicle-mounted self-contained odometer shall give high position accuracy for

SINS. The odometer assembly will have inductive proximity sensors, a proximity wheel with a sufficient number of serrations and readout electronics to generate sequential pulses in proportion to the vehicle speed. The exploded view of the odometer assembly is presented in Fig. 4(a). Two inductive proximity sensors equipped near the proximity wheel are used to differentiate the vehicle motion in forward and reverse direction by detecting the phase lead and phase lag from the pulse output of both the sensors as ODO_A and ODO_B as shown in Fig. 4(b). These pulses are converted to equivalent forward velocity through signal processing circuitry as shown in Fig. 4(c) through a Field Programmable Gate Array (FPGA) and in-house designed System-On-Chip (SOC) navigation processor. Placement of proximity sensors near to proximity wheel should be arranged in such a manner that both sensor output pulses should be in quadrature phase shift. State machine implemented in the SINS to detect vehicle motion and direction of movement is shown in Fig. 4(d) where one pulse rotation with a combination of two proximity sensors gives four different combinations of state outputs as 00, 01, 10 & 11. The processed output will be the number of pulses per sampling duration and the direction of wheel rotation (Forward/reverse) as per the state machine shown in Fig 4(d).

3.1 Selection Criteria of Scale Factor and Placement of Proximity Sensors

The objective is to obtain resolution in distance travelled $< \rho_r$ which is of navigation grade.

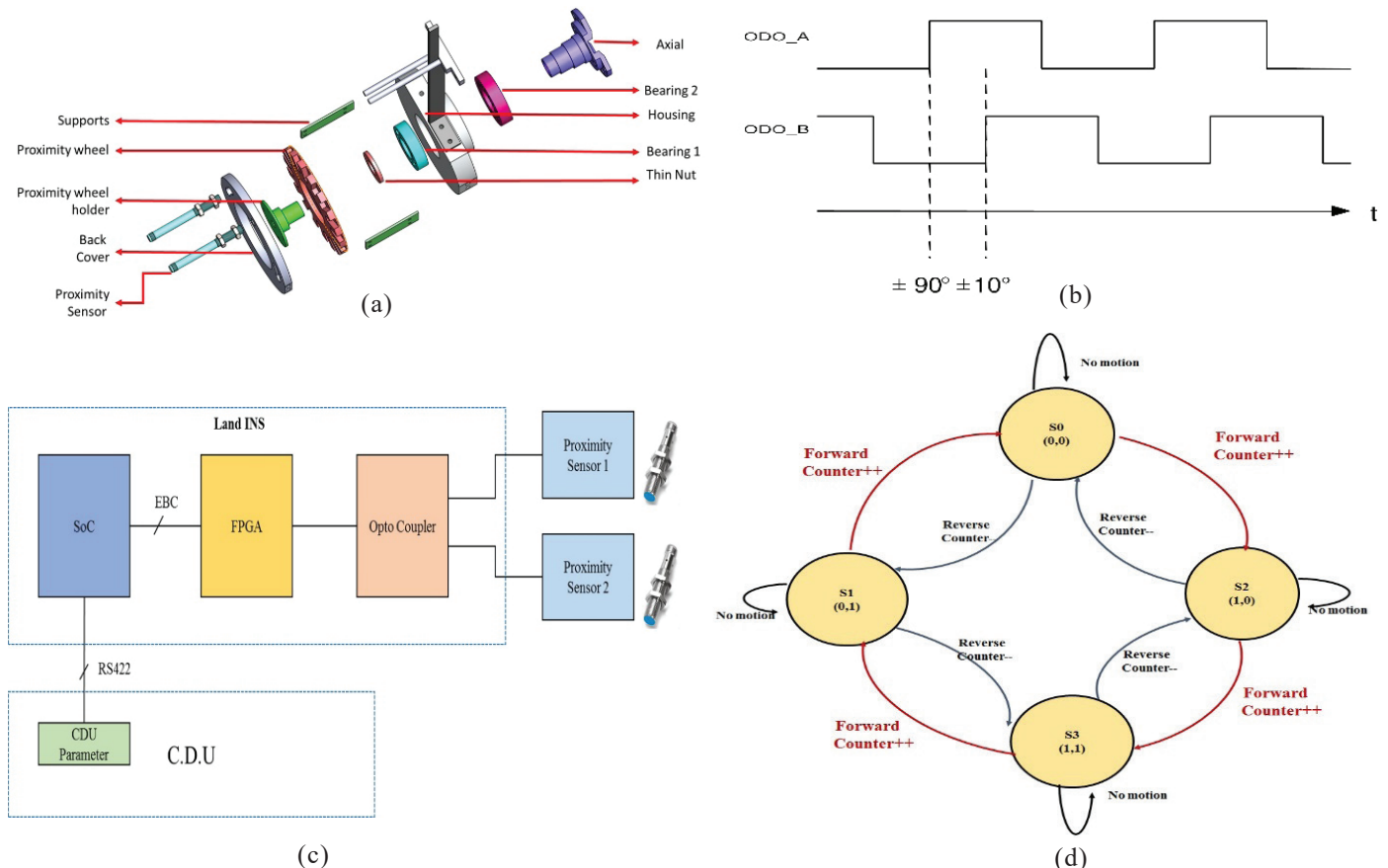


Figure 4. Odometer and its signal processing functions: (a) Odometer exploded view; (b) Quadrature phase shift sensor output; (c) Odometer signal processing circuitry; (d): State diagram for quadrature decoding.

3.1.1 Design Criteria

$$(\pi * D_w / N_w) < (\rho_r) \quad (11)$$

where,

D_w : Diameter of vehicle non-steering wheel

N_w : Pulse count per each revolution of the wheel.

Let D_w be 45 cms and the circumference of the vehicle wheel is $\pi * 45 = 141$ cm and the corresponding count to be obtained in one rotation of the wheel is N_w with $141 / N_w <$ resolution of 2 cm. Number of counts per rotation (N_w) should be greater than 70.68. Hence, N_w is chosen as 72. As a quadrature decoder is used at the detector circuit with 4 pulses output for each crossing of serration on the proximity wheel, the number of teeth required on the phonic wheel is 18 through $72/4$.

3.1.2 Design of Proximity Wheel

The diameter of the proximity wheel is chosen as 18 cm as it should be much less than the diameter of the wheel of the vehicle considering the mechanical mounting feasibility.

3.1.3 Placement of Proximity Sensors

Circumference of proximity wheel:

$$\pi * 18 \text{ cm} = 56.549 \text{ cm}$$

The displacement of 56.549 cm corresponds to one rotation of the vehicle wheel.

As the proximity wheel consists of 18 teeth, the displacement of $565.49 \text{ mm} / 18 = 31.42 \text{ mm}$ corresponds to the movement of the vehicle wheel for one tooth duration which in turn corresponds to electrical 360° in the sensor output as shown in Fig. 4(b). To obtain quadrature phase shift in the output of sensors w.r.t. each other, the minimum placement gap of proximity sensors should be:

$$31.42 \text{ mm} / 4 = 7.855 \text{ mm}.$$

The other possible sensor placement locations are governed by the relation:

$$7.855 \text{ mm} + (N \times 31.42 \text{ mm}) \quad (12)$$

where, $N = 0, 1, 2, 3, 4, 5, \dots, 17$

The optimum 'N' value may be chosen with regard to mechanical mounting feasibility for placement of proximity

sensor to obtain quadrature phase shift between outputs of 2 sensors. Finally, the ODO nominal scale factor shall be considered as $141 \text{ cm} / 72 \text{ pulses} = 0.0195 \text{ m/pulse}$.

3.2 Odometer Pulse Reading Implementation

Quadrature decoding logic is implemented in FPGA to obtain the required pulse count during motion and when the counter is not updating it indicates the vehicle is at rest. The pulse count represents the motion of the vehicle through the acceptable phase displacement of $\pm 90^\circ$ and indicates the direction: forward (ODO_A front before ODO_B front) or reverse (ODO_A front after ODO_B front). The proximity sensor being used in the odometer design is capable of detecting up to 1 KHz. To test the accuracy of the data reading algorithm, simulation was carried out in FPGA using the Xilinx tool ISE 14.1 version²¹. With the use of inductive sensors and a proximity wheel, the odometer delivers two pulse signals ODO_A and ODO_B in quadrature as shown in Fig 5(a).

3.3 Validation Scheme of Odometer Velocity

The designed odometer is connected to a calibrated rotor shaft mechanism and the corresponding quadrature phase shift pulses generated are fed as input to odometer signal processing circuitry to validate the scheme mentioned in Fig 4(c). Pulse count recorders running in FPGA are latched periodically and matched with the theoretical input angular speed of the shaft to validate the proposed scheme. The experimental test results of odometer pulses in quadrature phase are shown in Fig. 5(b).

4. SINS/ODOMETER BASED HYBRID NAVIGATION SCHEME

To fuse the data from the odometer and inertial sensors, an extended Kalman filter with a non-holonomic constraints (NHC) - based measurement model is devised and the corresponding error state vector $\delta X_f(t)$ of 18-dimension is defined as:

$$\delta X_f(t) = [\delta X_{INS}(t) \quad \delta X_{ODO}(t)]^T \quad (13)$$

where $\delta X_{INS}(t) = [(\delta p^n) \quad (\delta v^n) \quad (\delta \alpha^n)^T \quad (\delta \omega^b) \quad (\delta f^b)]^T$
 Position error vector $\delta p^n = [\delta \lambda_d \quad \delta L_d \quad \delta h_d]^T$

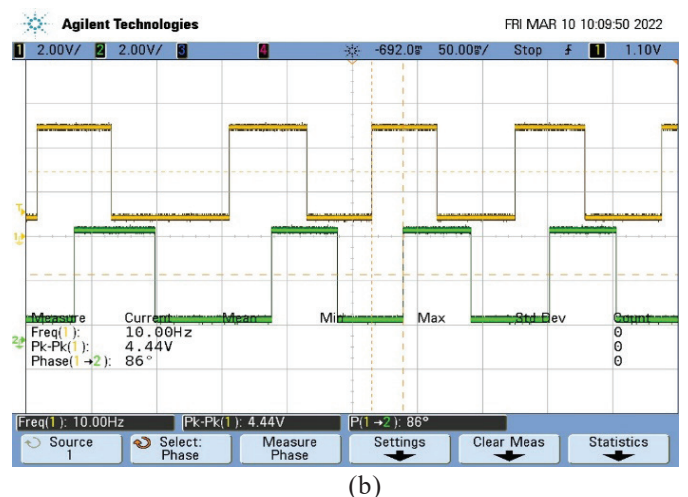
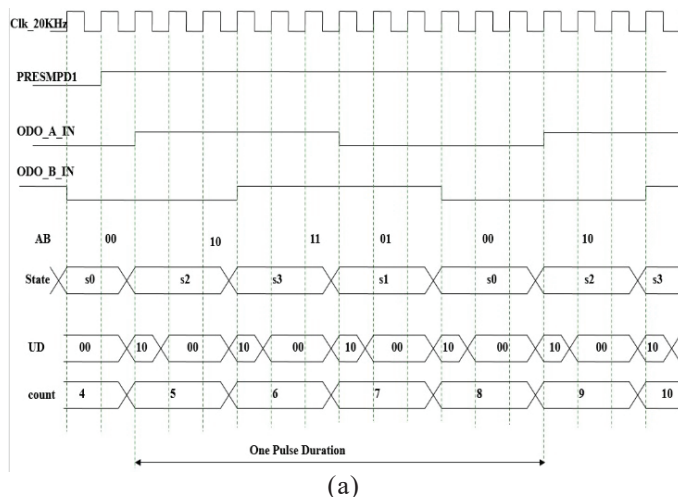


Figure 5. Odometer pulse reading implementation: (a) Simulation results for quadrature decoding in FPGA; (b) Measurements of odometer pulses through an oscilloscope.

Velocity error vector $\delta v^n = [\delta v_N \quad \delta v_E \quad \delta v_D]^T$

Angle error vector $\delta \alpha^n = [\delta \alpha_N \quad \delta \alpha_E \quad \delta \alpha_D]^T$

Gyro bias vector $\delta \omega_{ib}^b = [\delta \omega_x^b \quad \delta \omega_y^b \quad \delta \omega_z^b]^T$

Accelerometer bias vector $\delta f^b = [\delta f_x^b \quad \delta f_y^b \quad \delta f_z^b]^T$

- Position error linearized model

$$\delta \dot{p}^n = \phi_{pp} \delta p^n + \phi_{pv} \delta v^n + \phi_{p\alpha} \delta \alpha^n \quad (14)$$

where,

$$\phi_{pp} = \begin{bmatrix} 0 & 0 & \frac{-v_N}{(R_{Md})^2} \\ \frac{v_E \tan(\lambda_d)}{(R_{Nd}) \cos(\lambda_d)} & 0 & \frac{-v_E}{(R_{Nd})^2 \cos(\lambda_d)} \\ 0 & 0 & 0 \end{bmatrix}$$

$$\phi_{pv} = \begin{bmatrix} \frac{1}{(R_{Md})} & 0 & 0 \\ 0 & \frac{1}{(R_{Nd}) \cos \lambda_d} & 0 \\ 0 & 0 & -1 \end{bmatrix}$$

$$\phi_{p\alpha} = 0$$

- Velocity error linearized model

$$\delta \dot{v}^n = \phi_{vp} \delta p^n + \phi_{vv} \delta v^n + \phi_{v\alpha} \delta \alpha^n - dcm_n^b \delta f^b \quad (15)$$

where,

$$\phi_{vp} = 2 \begin{bmatrix} -2v_E \omega_N - \frac{v_E v_E}{(R_{Nd}) \cos^2(\lambda_d)} & 0 & \frac{-v_N v_D + v_E v_E \tan \lambda_d}{(R_{Md})^2} & \frac{v_E \tan \lambda_d}{(R_{Nd})^2} \\ 2(v_N \omega_N + v_D \omega_D) + \frac{v_N v_E}{(R_{Nd}) \cos^2(\lambda_d)} & 0 & \frac{-v_D v_E + v_N v_E \tan \lambda_d}{(R_{Nd})^2} & \frac{v_E \tan \lambda_d}{(R_{Nd})^2} \\ -2v_E \omega_D & 0 & \frac{v_E^2 - 2g_d R_{Nd}}{(R_{Nd})^2} & \frac{v_N^2}{(R_{Md})^2} \end{bmatrix}$$

$$\phi_{vv} = \begin{bmatrix} \frac{v_D}{R_{Md}} & 2\omega_D + \frac{-2v_E \tan \lambda_d}{R_{Md}} & \frac{v_N}{R_{Md}} \\ -2\omega_D + \frac{v_E \tan \lambda_d}{R_{Nd}} & \frac{v_D + v_N \tan(\lambda_d)}{R_{Nd}} & 2\omega_N + \frac{v_E}{R_{Nd}} \\ -2\frac{v_N}{R_{Md}} & -2\omega_N - \frac{2v_E}{R_{Nd}} & 0 \end{bmatrix}$$

$$\phi_{v\alpha} = \begin{bmatrix} 0 & f_d & -f_E \\ -f_D & 0 & f_N \\ f_E & -f_N & 0 \end{bmatrix}$$

- Attitude error linearized model

$$\delta \dot{\alpha}^n = \phi_{\alpha p} \delta p^n + \phi_{\alpha v} \delta v^n + \phi_{\alpha \alpha} \delta \alpha^n + [dcm]_n^b \delta \omega_{ib}^b \quad (16)$$

where

$$\phi_{\alpha p} = \begin{bmatrix} -\omega_D & 0 & \frac{V_E}{(R_{Nd})^2} \\ 0 & 0 & \frac{V_N}{(R_M)^2} \\ \omega_N + \frac{V_E}{(R_{Nd}) \cos^2(\lambda_d)} & 0 & \frac{V_E \tan(\lambda_d)}{(R_{Nd})^2} \end{bmatrix}$$

$$\phi_{\alpha v} = \begin{bmatrix} 0 & \frac{-1}{R_{Nd}} & 0 \\ \frac{1}{R_{Md}} & 0 & 0 \\ 0 & \frac{\tan(\lambda_d)}{R_{Nd}} & 0 \end{bmatrix}$$

$$\phi_{\alpha \alpha} = \begin{bmatrix} 0 & \omega_D - \frac{v_E \tan(\lambda_d)}{R_{Nd}} & \frac{v_N}{R_{Md}} \\ -\omega_D + \frac{v_E \tan(\lambda_d)}{R_{Nd}} & 0 & \omega_N + \frac{v_E}{R_{Nd}} \\ \frac{-V_N}{R_{Md}} & -\omega_N - \frac{v_E}{R_{Nd}} & 0 \end{bmatrix}$$

δf^b and $\delta \omega_{ib}^b$ are considered as random constants and are represented by:

$$\delta \dot{f}^b = 0 \quad (17)$$

$$\delta \dot{\omega}_{ib}^b = 0 \quad (18)$$

The composite error state equation from Eqn. (14-18) is written as:

$$\begin{bmatrix} \delta \dot{p}^n \\ \delta \dot{v}^n \\ \delta \dot{\alpha}^n \\ \delta \dot{\omega}_{ib}^b \\ \delta \dot{f}^b \end{bmatrix} = \begin{bmatrix} \phi_{vp} & \phi_{vv} & \phi_{v\alpha} & -[dcm]_n^b & 0 \\ \phi_{\alpha p} & \phi_{\alpha v} & \phi_{\alpha \alpha} & 0 & [dcm]_n^b \\ 0 & 0 & 0 & 0 & 0 \\ 0 & 0 & 0 & 0 & 0 \end{bmatrix} \begin{bmatrix} \delta p^n \\ \delta v^n \\ \delta \alpha^n \\ \delta \omega_{ib}^b \\ \delta f^b \end{bmatrix} \quad (19)$$

The above Eqn. (19) is represented in short form:

$$\delta \dot{X}_{INS}(t) = \phi_{INS} \delta X_{INS}(t) + v(t) \quad (20)$$

The measurement Eqn. for position and velocity measurements²² is:

$$\begin{bmatrix} \Delta p^n \\ \Delta v^n \end{bmatrix}_{6 \times 1} = \begin{bmatrix} [I_{3 \times 3}] & [0_{3 \times 3}] & [0_{3 \times 9}] \\ [0_{3 \times 3}] & [I_{3 \times 3}] & [0_{3 \times 9}] \end{bmatrix}_{6 \times 15} \begin{bmatrix} \Delta p^n \\ \Delta v^n \\ \Delta \alpha^n \\ \Delta \omega_{ib}^b \\ \Delta f^b \end{bmatrix}_{15 \times 1} \quad (21)$$

In case of GNSS absence, position and velocity measurements will not be available and hence proposed to have an alternative measurement from an odometer as a velocity-aiding sensor.

- Augmented state vector

$$\delta X_{ODO}(t) = [\delta s_{ODO} \quad \delta \beta_y \quad \delta \beta_z]^T \quad (22)$$

where, δs_{ODO} is the odometer scale factor error, $\delta \beta_y$ and $\delta \beta_z$ are pitch and azimuth misalignment angles of the odometer sensor with reference to the SINS body frame and corresponding error state-space model is:

$$\delta \dot{s}_{ODO} = 0 \quad (23)$$

$$\delta \dot{\beta}_y = 0 \quad (24)$$

$$\delta \dot{\alpha}_z = 0 \quad (25)$$

State-space model for the odometer integrated system from Eqn. (13) and Eqn. (19) is:

$$\delta \dot{X}_F(t) = \begin{bmatrix} \phi_{INS} & 0_{15 \times 3} \\ 0_{3 \times 15} & 0_{3 \times 3} \end{bmatrix} \delta X_F(t) + v(t) \quad (26)$$

And the corresponding state-transition matrix $\phi_{k/k-1}$ is expressed as: β

$$\phi_{k/k-1} = I + \phi_{INS} * \Delta T + \frac{\phi_{INS} * \Delta T^2}{2} \dots \quad (27)$$

Where, ΔT is an update interval for EKF and $v(t)$ represents the process noise. Further, the odometer measurement Eqn. is given by

$$Z_{odo} = \tilde{v}_{INS}^n - \tilde{v}_{ODO}^n = H_{odo} \delta X_F(t) + \xi(t) \quad (28)$$

The non-holonomic constraints (NHC) based lateral and vertical axes incremental velocities in the odometer sensor frame are assumed to have zero mean with Gaussian noise²³. Finally, the measurement equation is framed as:

- Measurement matrix

$$H_{ODO} = \begin{bmatrix} 0_{3 \times 3} & C_{ODO_{3 \times 3}}^n & 0_{3 \times 9} & M_v^{ODO} \end{bmatrix} \quad (29)$$

where

$$M_v^{ODO} = \begin{bmatrix} v_f^{ODO} & 0 & 0 \\ 0 & 0 & -v_f^{ODO} \\ 0 & v_f^{ODO} & 0 \end{bmatrix}$$

$C_{ODO_{3 \times 3}}^n$ is the transformation matrix from 'n'-frame to odometer frame, $\xi(t)$ represents the measurement noise; v_f^{ODO} is the odometer measured forward velocity in odometer frame and the SINS/odometer integration scheme is shown in Fig. 3.

4.1 Implementation of EKF

The propagated error state vector $(\delta X_F)_k^-$ and predicted error state covariance P_k^- are:

$$(\delta X_F)_k^- = \phi_{k/k-1} (\delta X_F)_{k-1} \quad (30)$$

$$P_k^- = \phi_{k/k-1} P_{k-1} \phi_{k/k-1}^T + Q_{k-1} \quad (31)$$

The updated Kalman gain matrix K_k , error state vector $(\delta X_F)_k$, and the error covariance matrix P_k are as follows:

$$K_k = P_k^- H_k^T (H_k P_k^- H_k^T + R_k)^{-1} \quad (32)$$

$$(\delta X_F)_k = (\delta X_F)_k^- + K_k (Z_k - H_k (\delta X_F)_k^-) \quad (33)$$

$$P_k = (I - K_k H_k) P_k^- \quad (34)$$

where $\phi_{k/k-1}$ is the state transformation matrix as shown in Eqn (27); H_k is the measurement matrix as shown in Eqn. (29) at k^{th} instance¹⁶. Measurement covariance of R_k for odometer is set as 0.01 (m/s)², the error covariance of P_k for position = diag(10m²), velocity = diag(0.15m/s)², angles = diag(1 mrad²), gyro bias = diag(10e-11 (rad/sec)²), accelerometer bias = diag(10e-8 (m/s/s)²).

5. FIELD TRIAL RESULTS

The objective of the field trial is two fold:

- To validate the proposed hybrid navigation scheme based on INS+ODOMETER data fusion.
- To study the inconsistency of GPS measurements during obstruction.

5.1 Test Results

To test the performance of the data fusion algorithm as explained in section 4, a proximity wheel is realized as per the design mentioned in section 3. In-house designed navigation grade 0.01 deg/hour class gyroscopes and 30 micro g class of

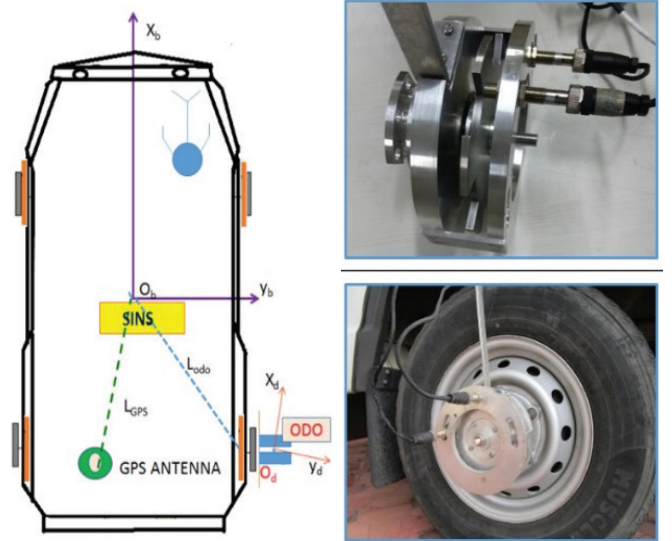


Figure 6. Sensor mounting locations (left) and odometer assembly on vehicle wheel (right).

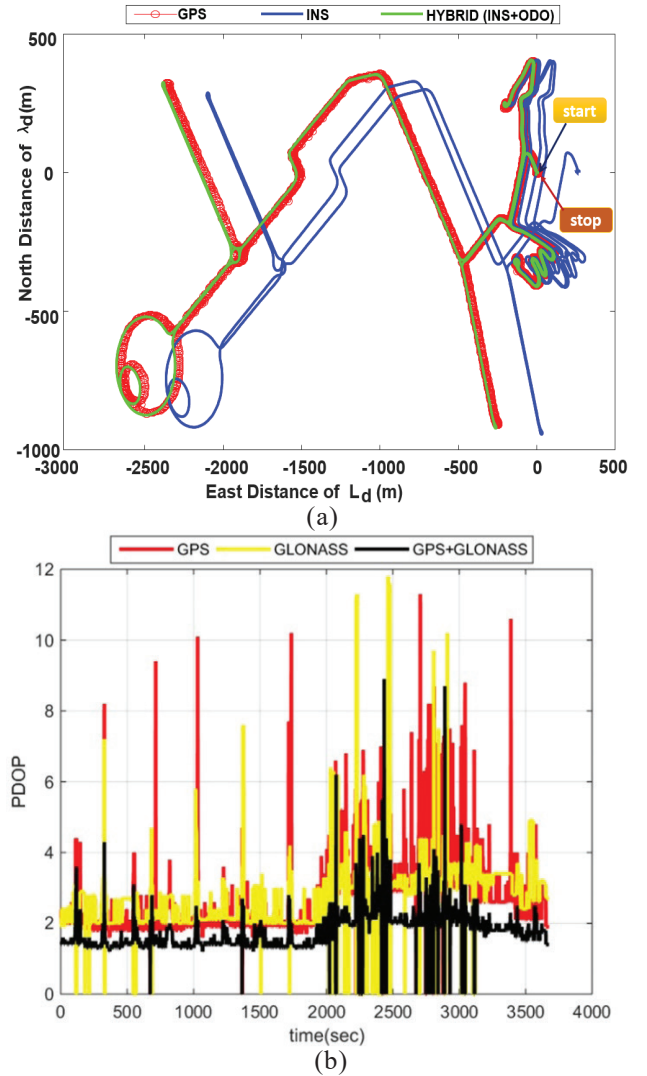


Figure 7. Motion path of vehicle and GPS signal availability: (a) Position generated by INS (un-damped), GPS, and proposed hybrid navigation computations; (b) Position dilution of precision (PDOP) as measured by GNSS receiver.

accelerometers are used to build SINS. Proximity wheel along with 2 proximity sensors of M/s. SICK with part number: p235529 is mounted on the rear wheel of the mobile van as shown in Fig. 6.

SINS installed within the van has an in-built GNSS receiver and a System-On-Chip (SOC) processor to implement the data fusion algorithm through an embedded real-time software module. After static initial Gyro-Compassing (GC) alignment, the van is moved within the technical campus and the corresponding profiles of motion path as generated by the pure INS (undamped), hybrid computations of INS and GPS are shown in Fig. 7(a).

Further, it can be noticed from Fig. 7(a), that the proposed hybrid navigation position track has closely followed the GPS-constructed path whereas the INS (undamped) computed position track is drifted by 350 mtr. It is to be noted that the INS (undamped) computed solution means, it is running in free inertial mode without any damping mechanism.

During the motion, the Position Dilution of Precision (PDOP) of GPS, GLONASS, and combined solution are presented in Fig. 7(b) which are poorer from 2000 seconds to 3200 seconds during the times when the vehicle moved through thick vegetation. This shows that the dilution of position information of GPS is not fully suitable for any kind of data fusion due to inconsistency in the 3D position fix. The odometer-measured pulses and its equivalent velocity along

the forward axis of the vehicle are compared with GPS and INS and shown in Fig. 8(a) and Fig 8(b). Fig. 8(c) presents the enlarged view of Fig. 8(b) from time 2000 sec to 3200 sec. Fig. 8(d) presents the zoomed view of forward velocity between 3590 sec to 3675 sec (vehicle is at rest from 3625 sec onwards).

When the vehicle is at rest, the zero velocity shall be the reference, and the errors in the velocity of pure INS is 0.22 m/sec whereas, the odometer computed velocity showing close to the zero line. The horizontal velocities as computed by INS (undamped), GPS, and the proposed hybrid scheme for data fusion between INS+ ODOMETER are presented in Fig. 9(a). The hybrid velocities are close to GPS-measured velocities after 1 hr of operation whereas, pure INS (un-damped) velocities are having drift of 0.2 m/s which can be seen in Fig. 9(b) during vehicle resting at the end of motion at 3640 sec.

The damped hybrid velocities as shown in Fig. 9(a) are achieved through 18 state EKF designed as presented in section 4. The odometer Scale Factor (SF) is initialized as 0.0195 meter/pulse and EKF could estimate the error of odometer SF by 0.06 % of the nominal scale factor as shown in Fig. 10.

Finally, the horizontal position error of the hybrid navigation solution (i.e. INS + ODO), when compared with the GPS solution, is shown in Fig. 11 and found within the accuracy of 10 m (RMS) at the end of 3675 sec. Also, the undamped position error through the INS solution is plotted in Fig. 11 for comparison with the damped hybrid position error.

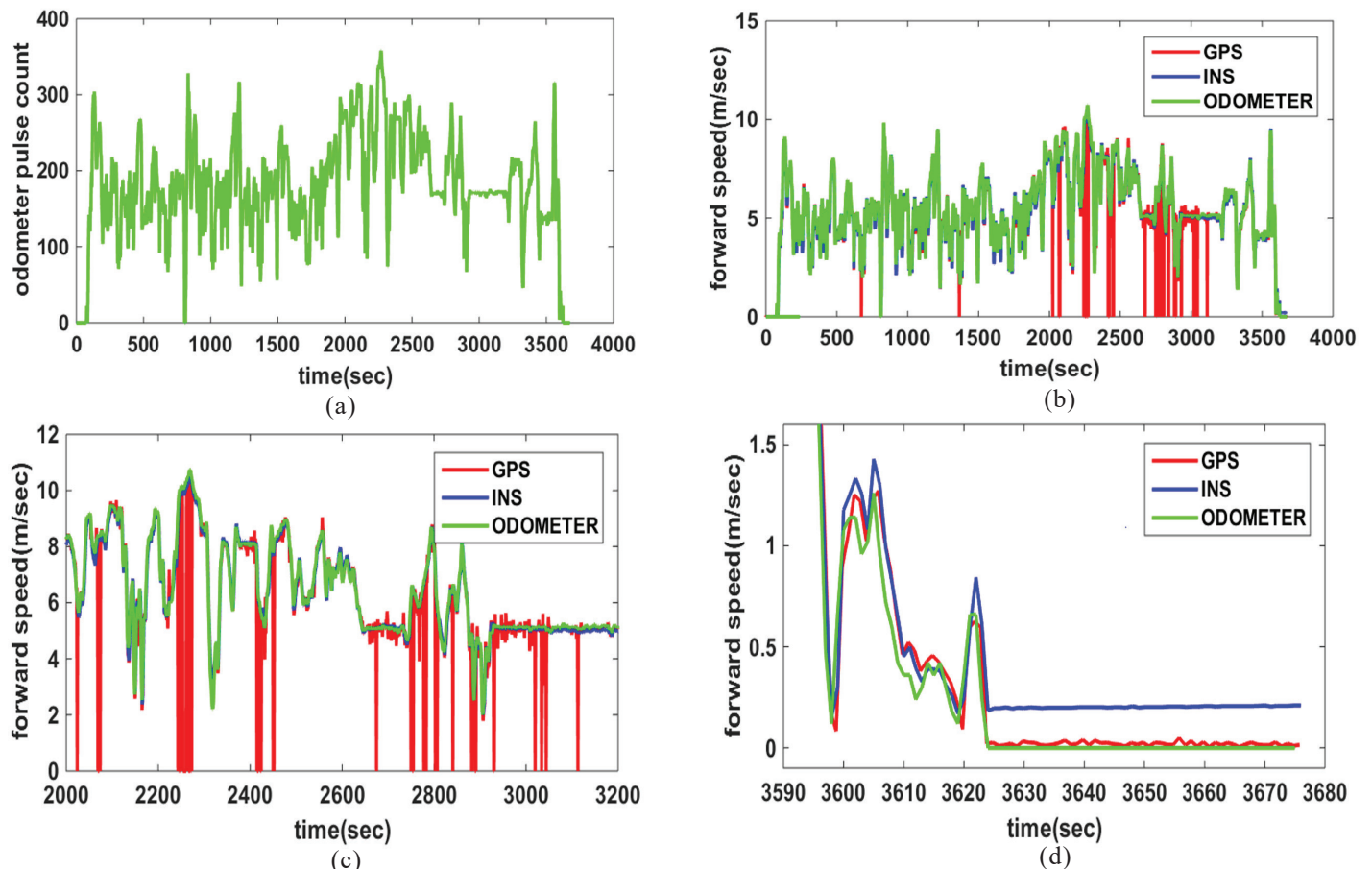


Figure 8. Odometer measurements & forward velocity (a) Odometer pulse count; (b) Forward velocity measured by GPS, INS & Odometer; (c) Forward velocity zoomed between 2000 sec to 3200 sec; (d) Forward velocity zoomed between 3590 sec to 3675 sec (the vehicle is at rest from 3625 sec onwards).

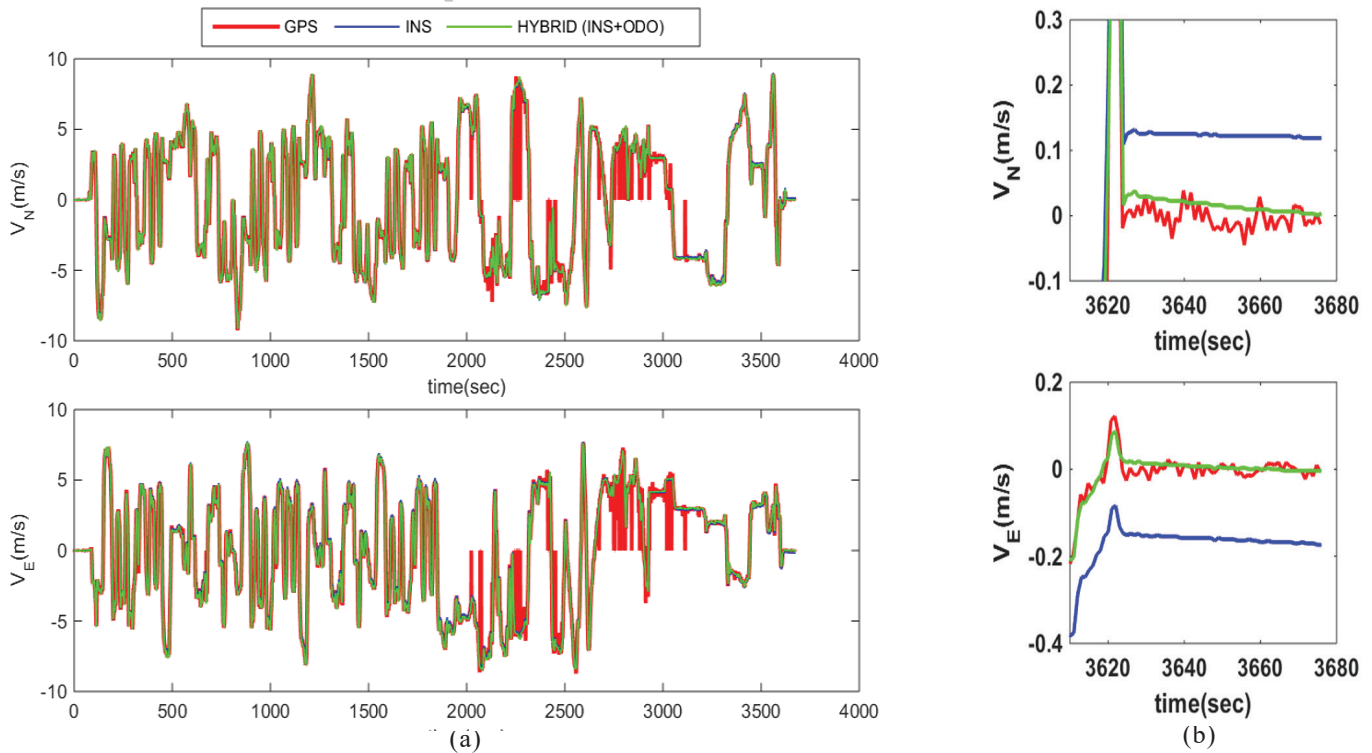


Figure 9. Horizontal velocities of GPS, INS, and proposed hybrid navigation computations (a) Full profile view (b) zoom view from 3610 sec to 3675 sec (vehicle is stopped at 3625 sec).

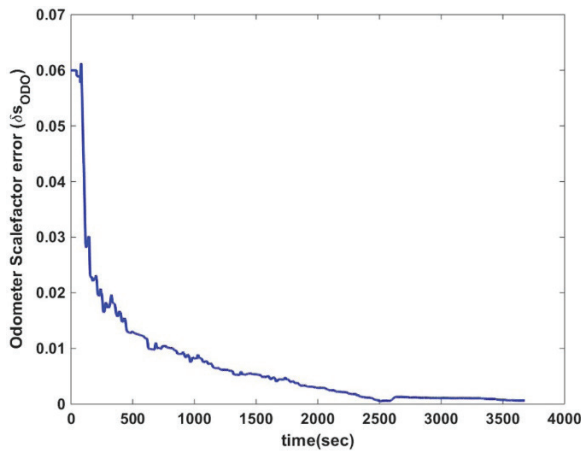


Figure 10. Estimated scale factor error of odometer

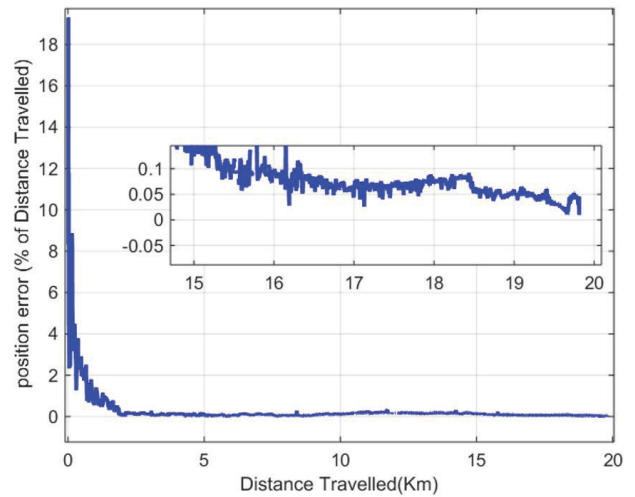


Figure 12. Hybrid horizontal (damped) error expressed as % of distance travelled (DT).

The error in the INS (undamped) position solution is found to be 350 mtr (peak) at 3000 sec and 290 mtr at the end of 3675 sec. Position errors of the hybrid navigation system over 1 hr of navigation with reference to a travelled distance of 20km is less than 0.05 % of distance travelled (DT) and is presented in Fig. 12.

Hence, the proposed hybrid navigation scheme can provide the required position accuracies of less than 10 mtr for a range of 20 km and 0.05 % of distance travelled beyond the range of 20 km under the GPS denial regime or compromised environments.

5.2 Discussion

In order to validate the performance of the proposed

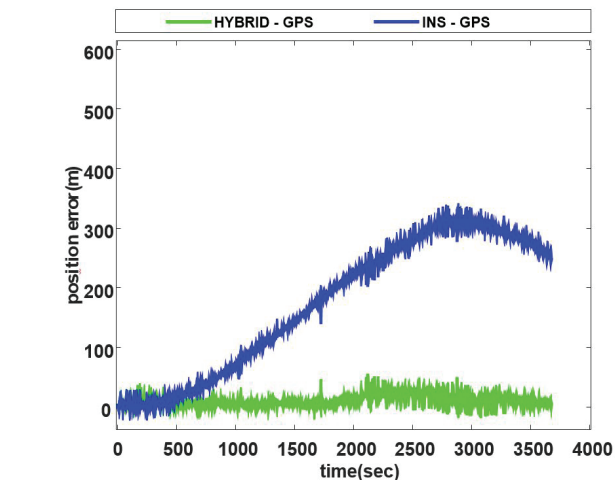


Figure 11. Horizontal position error of proposed hybrid and INS (un-damped) when compared with GPS.

hybrid navigation scheme with INS+ODOMETER, the SINS is initialized with pre-surveyed coordinates (start point) and brought back to the same point (stop point) at the end of test duration. Hence, the drifted errors of hybrid navigation computations can be easily judged with respect to common start/stop points. Further, during the motion, the embedded GPS receiver measurements shall be taken as a reference. However, the GPS measurements are found to be inconsistent during the time of obstruction. Hence, the following are the 3 scenarios considered towards evaluation of the proposed hybrid navigation scheme.

5.2.1 Scenario 1

Under normal operating conditions with the GPS antenna mounted on the top of the moving vehicle with a clear view to open sky, the GPS receiver shall be providing an accuracy of 10 m (RMS). Since GPS signals did not see any obstruction from 0 sec to 2000 sec, GPS is considered as a reference during static and dynamic motion conditions with 10 mtr (RMS) accuracy.

5.2.2 Scenario 2

GPS is not consistent from 2000 sec to 3200 sec. The GPS positioning accuracy was varying from 50 to 70 mtr with high PDOP and low C_p/N due to obstruction from thick vegetation and high-rise concrete structures around. It was found that the fix loss and regain were happening very frequently. Whenever GPS fix was available, the position coordinates were found to be very noisy varying around 50 mtr (non-Gaussian). Ideally, the GPS cannot be taken as an acceptable reference. However, comparing the large error of pure inertial drift rate of INS (undamped) which may go up to 350 mtr to 1 km, the GPS can be considered as the best available source of information with 50 mtr error (RMS) during the time from 2000 sec to 3200 sec.

5.2.3 Scenario 3

GPS is very consistent from 3200 sec to 3675 sec during the times when the antenna is fully exposed to open sky once again. Hence, the GPS shall act as a reference during the end phase of the test when the antenna is exposed to the open sky under motion and under vehicle parked conditions.

To summarize, we have GPS measurements available during dynamic motion with 10 mtr (RMS) accuracy under normal operating conditions and diluted accuracy of 50 mtr (RMS) during obstruction. Moreover, the accuracy of the proposed hybrid navigation scheme is validated with respective common start/stop points as provided by precise surveyed coordinates.

The problem of GNSS signal reception reported in the present manuscript is attributed to two factors: Case (a): GNSS is vulnerable to external factors and is not available due to complete blockage when the need is desperate in the battlefield. Case (b): The partial blockage of signal due to thick vegetation around or due to hideout in the combat mode. Hence, it is advised not to depend on GNSS signals for special/strategic operations. Multi-frequency GNSS receivers may provide improved position accuracy up to sub-meter level under normal operating conditions but are challenged by jamming

and spoofing or signal blockage during hideouts or strategic operations.

In view of the above, there is a need for alternative means of achieving required positioning accuracies, and authors in the present manuscript proposed to have an accurate hybrid navigation solution from SINS with the use of an odometer as an auxiliary sensor. This justifies the importance of the work reported in the present manuscript.

6. CONCLUSION

In this paper, a detailed design of a navigation grade SINS and fusion algorithm for the integration of inertial sensor data with odometer data has been presented. Van trials are carried out to validate the algorithms and implementation scheme. Results of SINS/Odometer integrated hybrid position error are comparable with the position errors with 10m accuracy during the times when GPS is available and consistent. Hence, it is shown that a navigation system with the proposed resilient feature, can give high position accuracy of less than 0.05 % of DT in GPS/GNSS denied environment for land vehicles. Further, fault detection like wheel skidding and sideslip can be added as additional states to improve upon the positioning accuracies which will be reported in future works.

REFERENCES

1. IEEE-STD-1559, *IEEE Stand. Inertial Syst. Terminol.*, 2022.
doi:10.1109/IEEESTD.2022.9961160
2. Titterton, D. & Weston, J. Strapdown inertial navigation technology, 2nd ed. London, U.K.: IET, 2004.
doi: 10.1049/PBRA017E
3. Azkarate, M.; Gerdes, L.; Joudrier, L. & Pérez-del-Pulgar, C.J. A GNC Architecture for planetary rovers with autonomous navigation. *In IEEE Int. Conf. on Rob. Autom. (ICRA)*, Paris, France, 2020, PP. 3003-09.
doi: 10.1109/ICRA40945.2020.9197122
4. Groves, P.D. Principles of GNSS, Inertial, and Multi-sensor Integrated Navigation Systems, 2nd ed. Norwood, MA, USA: Artech House, 2013.
5. Liu, Y.; Li, S.; Fu, Q.; Liu, Z.; & Zhou, Q. Analysis of kalman filter innovation-based GNSS spoofing detection method for INS/GNSS integrated navigation system, *IEEE Sens. J.*, 2019, **19**(13), 5167-78.
doi: 10.1109/JSEN.2019.2902178
6. Muralikrishna, G.; Malleshm, G. & Kannan, M. Autonomous integrity monitoring of INS/GPS integrated navigation system under multipath environment. *In 6th IEEE Int. Conf. on Electron. Commun. Aerosp. Technol.* Coimbatore, India, 2022, PP. 55-62.
doi: 10.1109/ICECA55336.2022.10009084
7. Chiang, K.W.; Chang, H.W.; Li, Y.H.; Tsai G.J.; Tseng, C.L.; Tien, Y.C. & Hsu, P. C. Assessment for INS/GNSS/odometer/barometer integration in loosely-coupled and tightly-coupled scheme in a GNSS-degraded environment. *IEEE Sens. J.*, 2020, **20**(6), 3057-69.
doi:10.1109/JSEN.2019.2954532
8. Jungi Park, J.G.; Lee, D.S. & Park, C. Implementation of vehicle navigation system using GNSS, INS, odometer

- and barometer. *J. Positioning, Navigation and Timing, JPNT*, 2015, **4**(3), 141-150.
doi:10.11003/JPNT.2015.4.3.141
9. Schütz, A.; Sánchez-Morales, D.E. & Pany, T. Precise positioning through a loosely-coupled sensor fusion of GNSS-RTK, INS and LiDAR for autonomous driving. *In IEEE/ION Position, Location and Navigation Symp. (PLANS)*, Portland, OR, USA, 2020, 219-225.
doi: 10.1109/PLANS46316.2020.9109934
 10. Yu, P.; Wei, W.; Li, J.; Wang, F.; Zhang, L.; & Chen, Z. An improved autonomous inertial-based integrated navigation scheme based on vehicle motion recognition, *IEEE Access*, 2023, **11**, 104806-16.
doi: 10.1109/ACCESS.2023.3318548.
 11. Farrell, J.A. *Aided navigation: With High Rate Sensors*, McGraw-Hill Publications, 2008.
 12. Wang, M.; Wu, W.; He, X.; Li, Y. & Pan, X. Consistent ST-EKF for long distance land vehicle navigation based on SINS/OD Integration. *IEEE Trans. on Vehicular Technol.*, 2019, **68**(11), 10525-34.
doi: 10.1109/TVT.2019.2939679
 13. Zhong, M.; Guo, J. & Yang, Z. On real-time performance evaluation of the inertial sensors for INS/GPS integrated systems. *IEEE Sens. J.*, 2016, **16**(17), 6652-61.
doi: 10.1109/JSEN.2016. 2588140
 14. Dissanayake, G.; Sukkarieh, S.; Nebot, E. & Durrant-Whyte, H. The aiding of a low-cost strap-down inertial measurement unit using vehicle model constraints for land vehicle applications. *IEEE Trans. Robot. Autom.* 2001, **17**(5), 731-47.
doi: 10.1109/70.964672
 15. Fu, Q.; Liu, Y.; Liu, Z.; Li, S. & Guan, B. High-Accuracy SINS/LDV Integration for long-distance land navigation. *IEEE/ASME Trans. Mechatron.* 2018, **23**(6), 2952-62.
doi: 10.1109/TMECH.2018. 2875151
 16. Klimkovich, B.V. Self-calibration of a digital odometer integrated with a three-component SINS for a Land vehicle. *In IEEE 24th Saint Petersburg Int. Conf. Integr. Navigation Syst. (ICINS)*, 2017, 1-4.
doi:10.23919/ICINS.2017. 7995639
 17. Wu, Y.; Wu, M.; Hu, X. & Hu, D. Self-calibration for land navigation using inertial sensors and odometer: observability analysis. *In AIAA GNC Conference*, 10 - 13 August 2009, Chicago, Illinois.
doi:10.2514/6.2009-5970
 18. Vasilyuk, N. & Tokarev, D. Identification of geometric displacements of odometers in a GNSS/inertial navigation system installed on a land vehicle. *IEEE/ION PLANS*, Portland, OR, USA, 2020, 197-207.
doi: 10.1109/PLANS46316. 2020.9110193
 19. Wang, L.; Niu, X.; Zhang T.; Tang, H. & Chen, Q. Accuracy and robustness of ODO/NHC measurement models for wheeled robot positioning. *Meas.*, 2022, **201**, 111720.
doi: 10.1016/j.measurement.2022.111720
 20. Wu, Y.; Niu, X. & Kuang, J. A comparison of three measurement models for the wheel-mounted MEMS IMU-based dead reckoning system. *IEEE Trans. on Veh. Technol.*, 2021, **70**(11), 11193-203.
doi: 10.1109/TVT.2021. 3102409
 21. <https://www.xilinx.com/downloadNav/vivado-design-tools/archive-ise.html> for Xilinx Tool, ISE 14.1. (Accessed on 14 April, 2024)
 22. Reddy, G. & Saraswat, V.K. Advanced navigation system for aircraft applications. *Def. Sci. J.*, 2013, **63**(2), 131-137.
doi: 10.14429/dsj.63.4254
 23. Gelb, A. *Applied optimal estimation*. MIT Press, Cambridge, May 15, 1974.

ACKNOWLEDGEMENT

The authors are thankful to Dr. Anindya Biswas, Director, RCI and Dr. U Rajababu DG(MSS) for their continuous support and monitoring of the development work. Also, the authors are indebted to M. Kannan, Director of Navigation Systems, Dr. BHVS Narayanamurthy, former DG(MSS) and Dr. G Satheesh Reddy, Former Secretary, DD R&D for preliminary conceptualization and building of supporting infrastructure for land navigation system development.

CONTRIBUTORS

Mr G. Muralikrishna obtained his MTech in Electrical Engineering from IIT Delhi. He is working as a Scientist at DRDO-RCI, Hyderabad. His areas of research include: Inertial navigation systems & satellite navigation systems for various flight vehicle applications also the development of smart navigation, redundant navigation systems and multi-sensor data fusion for various flight vehicles.

In the current study, he conceptualised the design of the odometer as a navigation-aid for the present manuscript and devised the hybrid navigation algorithm

Dr G. Mallesham obtained his PhD degrees from the Electrical Department, IIT, Delhi. He is currently working as a Professor in the Department of Electrical Engineering, University College of Engineering, Osmania University. His research interest include: System modeling, control and automation, soft computing, renewable energy, smart micro grid, smart navigation and multisensory data fusion.

In the current study, he guided the overall design of the hybrid navigation mechanism along with sensor noise characterisation and observability analysis of the present work reported.

Mr Abhishek Jain obtained BTech in Computer Engineering from NIT Surat. He joined as Scientist at RCI/DRDO. His areas of interest include: Design and development of Real-time embedded software for multi-sensor-fusion applications. In the current study, he designed the real-time navigation software for the work presented and carried out the field testing.

Mr Praveen Tiwari obtained his BTech from VNR VJIET, JNTU, Hyderabad and joined as a Scientist at RCI/DRDO. His areas of interest include: Design and development of sensor processing electronics and digital navigation electronics. In the current study, he designed the odometer electronics circuitry along with FPGA implementation.